Title

LAYER GROWTH AND MICROSTRUCTURE IN Nb3Sn MULTIFILAMENTARY SUPERCONDUCTING WIRE

Author

Tribula, D.

Publication Date

1986-05-01

LBL-21729

LAYER GROWTH AND MICROSTRUCTURE IN Nb_3Sn MULTIFILAMENTARY SUPERCONDUCTING WIRE

D. Tribula
(M.S. Thesis)

May 1986

Lawrence Berkeley Laboratory
University of California
Berkeley, California 94720

Prepared for the U.S. Department of Energy
under Contract DE-AC03-76SF00098

Center for Advanced Materials

DISCLAIMER

LBL-21729

LAYER GROWTH AND MICROSTRUCTURE IN Nb_3Sn MULTIFILAMENTARY SUPERCONDUCTING WIRE

Dana Tribula
M.S. Thesis

Department of Materials Science and Mineral Engineering
University of California

and

Center for Advanced Materials
Lawrence Berkeley Laboratory
University of California
Berkeley, California 94720

May 1986

ACKNOWLEDGEMENT

Special thanks are extended to Professor J.W. Morris, Jr., J.W. Chan, D.R. Dietderich, and P.E. Johnson for continued support and critical discussion. This work was supported by the Director, Office of Energy Research, Office of Basic Energy Sciences, Materials Science Division, U.S. Department of Energy under contract no. DE-AC03-76SF00098. The critical current measurements were made at the Francis Bitter National Magnet Laboratory.

I. INTRODUCTION

Multifilamentary Nb_3Sn conductors are strong candidates for use in high-field superconducting magnet systems, such as those proposed for fusion reactors and high-energy particle accelerators. Generation of these high fields requires high currents in the magnet windings. A factor influencing the current carrying capacity of Nb_3Sn conductors, as well as all type II superconductors, is their microstructure. Thus, optimization of the microstructure is one method of increasing the maximum current that such a conductor can carry. For effective microstructural control, it is necessary to understand the microstructural development of the Nb_3Sn superconducting phase, and to identify the factors that are influential in its development.

The maximum current density that can be carried by a superconductor is the critical current density (J_c), which is a function of the temperature and applied external field. The J_c is one of three critical parameters that defines the superconducting state. The others are the critical temperature (T_c) and the upper critical field (H_{c2}). These parameters are determined by the composition and crystallographic order, the microstructure, and the state of strain. The composition and order determine the inherent superconducting properties; the state of strain of the superconducting phase, resulting from the macrostructure of the conductor, modifies these inherent properties. The microstructure determines the density of flux line pinning sites which prevent the loss of superconductivity under the passage of a transport current. The primary pinning sites in Nb_3Sn superconductors are grain boundaries (1-5).

Of the three interdependent critical parameters, the upper critical field most accurately reflects the inherent material character, i.e. the "quality" of the superconductor regardless of its microstructure (6-8). The direct measurement of the upper critical field requires very high fields. (The upper critical field of Nb_3Sn is 23T at 4.2K). An approximate value for the upper critical field, called H_{c2}^*, is possible based on an analysis of $J_c(H)$ behaviour (9-12). Values of H_{c2}^* are conservative estimates of H_{c2}, and are useful in making conductor comparisons when high field data are not available.

Due to the brittle nature of the Nb_3Sn phase, specialized techniques have been developed for its fabrication into a conductor. The most widely used method is the "bronze process" (13). Pure Nb rods in a Cu-Sn matrix are deformed into the final desired conductor geometry. A reaction treatment at high temperature permits the diffusion of Sn from the matrix to the Nb filaments where the Nb and Sn react to form Nb_3Sn, Fig. (I-1) (32).

The microstructural state of the superconducting phase is indirectly determined by the starting geometry of the conductor, its processing history and subsequent reaction treatment. Optimized heat treatments that maximize the J_c for a specific conductor have been developed. However, a clear understanding of how and why a particular microstructure develops in a particular conductor has been lacking.

Recent work attributes the final microstructure to a competition between nucleation of new grains and growth of existing grains (17). An alternate hypothesis cites the induced stresses that develop during Nb_3Sn formation as the cause for the observed Nb_3Sn microstructure (18-21). The present work tests these hypotheses by direct observation of

the microstructural development in several dissimilar conductors.

Wires at various stages of reaction are monitored for amount of the Nb_3Sn phase formed and its microstructural state. The rate of Nb_3Sn formation is determined by the availability of Sn and is thus correlative with the known starting Sn supply and the observed microstructural evolution. Results presented here show a correspondence between the Nb_3Sn formation rate and the final grain structure.

In addition to optimization of the microstructure, it is possible to improve the J_c in multifilamentary Nb_3Sn conductors by the addition of third elements, Mg (22-24) and Ti (25-28). The combined effect on J_c of changes in the growth rate and third element additions is also assessed.

II. EXPERIMENTAL PROCEDURE

A. Sample Preparation

i. LBL wire

The multifilamentary wires are manufactured from pure starting materials. High purity copper and tin, in proportions to yield a 6.7at% Sn solution, are encapsulated in argon filled quartz tubes, melted and cast into rods. Any alloying additions to the bronze are added during the melting and casting process. The rods are homogenized (12 hours at 700°C) and swaged to a diameter of 1.4cm (0.53in) with intermediate annealing treatments (12 hours at 700°C) after each 40% reduction in cross-sectional area. Chemical analysis of samples taken along the length of the rod determines the Sn concentration profile.

Sn segregation will deleteriously affect further processing and final conductor performance. The analysis is performed commercially by Anamet Laboratories, Inc. of Berkeley, as well as at MMRD using x-ray fluorescence and x-ray emission techniques. The rods are machined into tubes of outer diameter with 1.1cm (0.45in) and inner diameter of 0.64cm (0.25in).

Pure Nb powder is compacted, sintered and swaged to a final outer diameter of 0.64cm (0.25in). This method of fabrication allows for easy alloying of the Nb. The Nb rod is inserted into the bronze tube and the composite is swaged and finally drawn to a diameter of 0.017cm (0.067in). The final draw is made through a hexagonal die to facilitate subsequent packing. Seven lengths of this monofilament are packed into a second bronze tube. The composite is swaged and drawn. Nineteen lengths of the resultant seven-filament wire are packed into the final bronze tube. This composite is again swaged and drawn to a final wire diameter of ~0.051cm (0.020in). (The actual outer wire diameter is adjusted to yield a Nb filament diameter of $\sim 8 \times 10^{-4}$cm). The wire is annealed at 450-500°C for 40-60 minutes after each 30-35% reduction in cross-sectional area to eliminate the work hardening in the matrix. The final cross-section of the wire contains nineteen bundles of seven filaments (a total of 133 Nb filaments) Fig.(II-1).

The finished wire is sectioned into 10cm lengths which are sealed in argon-filled quartz tubes and reacted at high temperature to form the Nb_3Sn superconducting phase. Reaction temperatures are at 700°C, 750°C, and 780°C for times ranging from 30 minutes to fourteen days. Each length provides three 3cm specimens for J_c testing.

ii. Hitachi wire

This is a commercially produced conductor, obtained from Hitachi, Ltd., Japan. The conductor contains 10,261 (31 bundles of 331) Nb filaments of $(3-4)\times10^{-4}$cm diameter in a 7.5at% Sn matrix. Each bundle of 331 filaments is wrapped in a Nb diffusion barrier, and the 31 bundles are encased in a Cu stabilizer. The overall diameter of the wire is 0.12cm. Heat treatment of this conductor is as above.

All wire parameters are listed in Table I.

B. Characterization

The materials' parameters of interest are the absolute amount of Nb_3Sn formed, its formation rate, and its microstructure.

i. Progress of Reaction

The amount of Nb_3Sn is determined through optical and SEM examination of polished and etched wire cross-sections at various stages of reaction. Polished specimens are etched in a solution of 72% lactic acid, 9% HF, 9% H_2SO_4(conc.), 1% H_2O_2, balance H_2O for 15-30 seconds. This etchant reveals the reacted Nb_3Sn phase, the unreacted Nb, and the bronze matrix. (Specimens are mounted such that the wire axis is perpendicular to the polished surface.) Amounts of Nb and Nb_3Sn phases are determined by measuring the appropriate areas on SEM micrographs (using a digitizing tablet). Thus the relative extent of the reaction is determined, and the absolute amount of the Nb_3Sn phase and of any unreacted Nb is calculated. For each wire cross-section a number of filaments are measured to insure good statistics.

ii. Growth Rate of Nb_3Sn Layer

The Nb_3Sn layer thickness is measured on high (10kX) magnification micrographs. The layer thickness is plotted as a function of reaction time at the various reaction temperatures, yielding the value of the time exponent and rate constant in the growth law, $d=kt^n$ (d is the layer thickness, k the rate constant, t the time, and n the time exponent).

iii. Microstructure

Microstructural information is obtained through both TEM and SEM techniques. TEM specimens are prepared by mechanically grinding longitudinal sections of the wire to a thickness of ~ 0.008cm (0.003in). Several such lengths are mounted on standard 0.3cm TEM disks and ion milled: high angle, high current, high voltage (23°, 0.4μA, 7kV), until perforation, followed by several hours at low angle, low current, low voltage (12°, 0.2μA, 4kV), to insure a thin viewing region. These specimens are examined in a Phillips 301EM microscope at 100kV. The objective is to determine grain size and shape within the Nb_3Sn layer, and to establish a correspondence between features seen in the TEM and those seen in the SEM. Representative micrographs are analyzed using the line intercept method.

Microstructural information from the SEM is obtained through examination of fracture surfaces. A length of the wire is scored and pulled to fracture; the fracture surface is examined in an ISI DS-130 scanning electron microscope. The superconducting phase is readily discernible by its brittle-fracture appearance. Within the

superconducting phase, the fracture mode is predominantly intergranular: high magnification micrographs reveal grain shape and size and their corresponding distributions.

C. Superconducting Properties

All critial current measurements were conducted at the Francis Bitter National Magnet Laboratory, Cambridge, Massachusetts, using a standard, four-point probe technique. Specimens, 3cm long, are mounted transverse to the magnetic field whose intensity can be varied from 8 to 20T. The critical current (I_c) is defined as the current that produces a voltage of one microvolt across voltage taps placed 5mm apart (a two microvolt per centimeter criterion). At least two specimens were measured for each datum point. The critical current density, J_c, is calculated by dividing the overall critical current, I_c, by the cross-sectional area of the Nb_3Sn phase (as determined from SEM).

The upper critical field, H_{c2}, is determined according to the Kramer (9) extrapolation. A plot of $J_c^{1/2}H^{1/4}$ vs. H is extrapolated to zero $J_c^{1/2}H^{1/4}$, via a least squares fit. The resultant H value, called H_{c2}^*, is a conservative estimate of the real H_{c2} (12).

III. RESULTS

A. Microstructure

i. LBL control wire

A multifold morphology is observed for most reaction treatments.

The reacted layer is divisible into two distinct regions: a columnar layer near the unreacted Nb core and a layer of equiaxed grains located between the columnar layer and the Cu-Sn matrix.

For very thin layers, the columnar grains are very distinct. The equiaxed layer is also evident; the grain diameter is roughly equal to the short transverse dimension of the columnar grains for grains nearest the columnar layer, increasing in size with proximity to the Cu-Sn matrix, Fig. (III-1). Initial layer growth occurs as an increase in both the columnar and equiaxed regions. During layer growth the columnar grains remain directly at the Nb/Nb_3Sn interface. As the layer thickens, the aspect ratio of the columnar grains drops and grain size within the equiaxed layer increases. Again, grain diameter, for those grains nearest the columnar layer, is approximately equal to the short transverse length of the columnar grains. Figure (III-2) shows high and low magnification fractographs of two specimens: 700°C/6 hour and 700°C/12 hour treatments.

With further aging the columnar grains remain at the interface and continue to thicken. However, they appear to decompose since overall layer growth occurs through growth of the equiaxed layer. The volume fraction of columnar grains decreases until finally only equiaxed grains remain. Figure (III-3a) shows a partially reacted wire, ~80% reacted. The columnar grains have decomposed; only equiaxed grains are seen. This single-fold morphology persists through complete reaction, i.e. total consumption of Nb. Figure (III-3b) shows a fully reacted wire, reacted at 700°C for 7 days. All the Nb has been consumed to form the superconducting phase. The grain shape is equiaxed throughout the Nb_3Sn layer, as seen in both SEM, Fig. (III-

3b), and TEM, Fig. (III-3c), micrographs. Average Nb_3Sn grain size at full reaction, at 700°C, is $0.13x10^{-4}$cm.

Similar morphologies are observed at higher reaction temperatures. Early stages of the transformation exhibit a columnar layer directly at the Nb/Nb_3Sn interface. On continued layer growth the columnar layer decomposes; a fully reacted wire exhibits only equiaxed grains, Fig. (III-4). Columnar grains that form at higher reaction temperatures are thicker than those that form at lower temperatures (for the same extent of reaction), and equiaxed grain size is larger. For a fully reacted wire at 700°C average grain size is $0.13x10^{-4}$cm; a fully reacted wire at 780°C has an average grain size of $0.28x10^{-4}$cm.

ii. LBL doped wire

The microstructures of the doped wires, with Mg or Ti additions, are similar to those observed for the control wire. Thin layers exhibit a multifold morphology: columnar grains directly at the Nb/Nb_3Sn interface, with an equiaxed shell surrounding the columnar layer that extends out to the bronze matrix, Fig. (III-5). Again the extent of the columnar layer decreases with increasing layer thickness. Fully reacted wires possess an equiaxed microstructure, Fig. (III-6). Grain sizes in the fully reacted wires, doped and undoped, are qualitatively similar.

iii. Hitachi Wire

A short reaction-treatment wire is shown in Fig. (III-7). Columnar grains of high aspect ratio are observed directly at the Nb/Nb_3Sn interface. The adjoining layer is composed of equiaxed grains with

average grain size of 0.18×10^{-4}cm. On further reaction there is slight thickening of the columnar grains accompanied by grain growth within the equiaxed layer. Layer growth occurs as an increase in the volume of both the columnar and the equiaxed regions. Figure (III-8) shows a wire reacted at 700°C for 7 hours and a wire reacted at 700°C for 7 days. The latter treatment, 700°C/7 days, represents the maximum obtainable amount of the Nb_3Sn phase. Due to an inadequate Sn supply, further aging does not result in additional Nb_3Sn formation, but rather growth of existing grains. Throughout the Nb_3Sn layer growth the multifold morphology is preserved. Although the columnar grains coarsen with the progress of the transformation, they are as distinct for a fully reacted wire as they are for a partially reacted wire. Equiaxed grains coarsen as well.

Similar behavior is observed at higher reaction temperatures. Columnar grains at the Nb/Nb_3Sn interface are present from the outset of the transformation through maximum reaction. For the same extent of reaction, higher reaction temperatures yield coarser columnar grains and larger average grain size, Fig. (III-9). In all cases, for grains nearest the columnar layer, the short transverse dimension of the columnar grains is approximately equal to the equiaxed grain diameter.

The microstructural development in all wires studied is similar. The Nb_3Sn always grows as columnar grains into the Nb core; columnar grains are always present at the Nb/Nb_3Sn interface. The balance of the Nb_3Sn layer is composed of equiaxed grains. Initial Nb_3Sn layer growth occurs as an increase in the amount of both the columnar and equiaxed regions. The columnar grains appear to decompose and further layer

growth is seen as an increase in the thickness of the equiaxed region. In all cases, the equiaxed grains adjacent to the columnar layer have a grain diameter approximately equal to the short transverse dimension of the columnar grains. The extent of each morphological region is a function of wire, reaction time and temperature. In the case of the LBL wire, both undoped and doped, the columnar region completely disappears prior to full reaction, resulting in a uniform equiaxed morphology. Figures (III-10) and (III-11) are schematic representations of the observed Nb_3Sn layer growth in the LBL and Hitachi conductors, respectively.

B. SEM vs. TEM

Figure (III-12) shows an LBL wire at two different stages of reaction. Three morphological regions are visible: the columnar layer at the Nb/Nb_3Sn interface, the equiaxed central layer, and finally, the larger equiaxed-grain layer near the bronze matrix. Microstructural features in these TEM micrographs compare favorably with features seen in SEM images of the same samples, Fig. (III-2) and Fig. (III-3a). A further example is shown in Fig. (III-13). The specimen is a partially reacted Hitachi wire. A cross-sectional TEM view is compared with a cross-sectional SEM image. Columnar and equiaxed grains are readily observed in both; grain sizes are qualitatively the same. These data are representative and indicate good agreement between SEM and TEM techniques.

C. Nb_3Sn Layer Growth

i. LBL control wire

The Nb_3Sn formation rate is monitored through measurement of the Nb_3Sn layer thickness (d) as a function of reaction time (t). A power growth law of the form $d=kt^n$ is assumed.

Layer thickness vs. reaction time is plotted for the LBL control wire in Fig. (III-14). Data for high and low temperature treatments, 700°C and 780°C, are shown. The lower temperature treatment data shows a slope of 0.5-0.6. The 780°C data show an n value of 0.6. The behavior of the doped wires is similar to that of the control wire (shown in scatter band in same figure).

Additionally, growth of the superconducting phase is measured through the use of the total reacted area. The percent reaction of a specimen is defined as the reacted Nb_3Sn area divided by the total active area (the sum of the unreacted Nb core area and the reacted Nb_3Sn area). The time to fully react a wire ranges from 2 to 7 days at 700°C and from 6 to 20 hours at 780°C, table II. The undoped wire has the slowest reaction rate at all temperatures; the Ti-doped wire reacts the fastest.

ii. Hitachi wire

A plot of layer thickness vs. reaction time is shown in Fig. (III-14a). The value of the time exponent is 0.2. This same slope is observed through full layer growth.

An insufficient Sn supply prevents the full consumption of Nb. The maximum percent reaction achieved is 70% after 7 days at 700°C and 70%

after 5 days at 750°C.

A comparison of the reaction rates of the LBL wires and the Hitachi wire reveals that the LBL wires, both undoped and doped react significantly faster than the Hitachi wire. Fifty percent reaction of the LBL wires is realized after 3 and 12 hours at 750°C and 700°C respectively; the Hitachi wire requires 12 hours at 750°C and 3 days at 700°C for the same extent of reaction, table II.

D. Effect of Dopants

The superconducting properties determined are the critical current density, J_c, and the upper critical field, H_{c2}^*. The J_c of the control, Ti-doped, and Mg-doped wires is shown as a function of reaction time at 700°C and 14T in Fig. (III-15). The peak J_c of the control wire at 14T is $2.3 \times 10^4 A/cm^2$. The upper critical field as extrapolated from a Kramer plot is ~18T, Fig. (III-16).

The Ti-doped wire has the best properties overall. The J_c increases by a factor of three at high fields over that of the control wire, $6.2 \times 10^4 A/cm^2$ vs. $2.3 \times 10^4 A/cm^2$ at 14T. This increase in J_c is accompanied by an increase in the H_{c2}^*, from 18T to 23T, as shown in Fig. (III-16).

The critical current densities of the Mg-doped wire are comparable to those of the control wire Fig. (III-15). The extrapolated upper critical field for this wire is estimated at slightly less than 18T, Fig. (III.16).

IV. DISCUSSION

A. Layer Growth

Growth of the Nb_3Sn layer occurs by diffusion of Sn through the matrix and the existing Nb_3Sn layer, to the Nb/Nb_3Sn interface (14-16,29). Here the Sn reacts with the remaining Nb to form additional Nb_3Sn. (Hence the direction of the layer growth is towards the center of the Nb filament.) The driving force for Sn diffusion is the chemical potential gradient that exists between Sn in the matrix and Sn in the Nb_3Sn. Holding other parameters constant, the greater the Sn concentration in the matrix, the steeper this gradient and the larger the driving force for Sn diffusion. Hence, a high concentration of Sn in the matrix results in a high Sn flux to the reaction front and a fast Nb_3Sn layer growth.

Table I lists several wire parameters of the samples studied. All LBL wires are similar, and they differ markedly in several respects from the Hitachi wire. Specifically, the bronze to niobium ratio (R) of the Hitachi wire is significantly less than the corresponding LBL value, R~3 and R~20, respectively. The matrix Sn concentration of the Hitachi wire is higher than that of the LBL wires, 7.4at% vs. 6.7at%, respectively. However, the much higher R value of the LBL wire results in a much larger net Sn supply.

As Nb_3Sn forms, the matrix Sn concentration drops and the driving force for further Sn diffusion to the Nb filaments is reduced. The LBL wires have a very high Sn supply and, even on full Nb conversion to Nb_3Sn, Sn depletion in the matrix is not severe. The Hitachi wire, on the other hand, has a much lower initial Sn supply and, as Nb_3Sn forms

Sn in the matrix is severely depleted. In this case, the driving force for Sn diffusion is greatly reduced as the reaction progresses.

This agrees with experimental observations. The high-Sn LBL wire reacts considerably faster than the low-Sn Hitachi wire, table II. Complete consumption of the Nb core occurs after 6 days/700°C for the LBL wire compared to >8 days/700°C to yield only 80% Nb conversion to Nb_3Sn in the Hitachi wire. In all wires, Nb_3Sn layer growth is fastest at the outset of the transformation, gradually decreasing as the reaction progresses. The last amount of Nb requires the longest time to react.

The rate of Nb_3Sn layer formation can be described by a power growth relationship. The value of the time exponent (n) indicates the rate limiting mechanism in the layer growth. An n value of 0.5 implies that the diffusion of the reacting species to the reaction front, i.e. Sn to Nb/Nb_3Sn, is the limiting step. If layer thickness is linearly proportional to time, n=1, the reaction itself is the slowest step in the transformation.

In these composite materials, three distinct processes are involved in the formation of Nb_3Sn. Sn diffusion through the matrix, Sn diffusion through the existing Nb_3Sn layer, and, finally, Sn reaction with Nb to form Nb_3Sn. The n value changes accordingly. A low n value, $n<0.5$, applies when the transformation is limited by Sn diffusion through the matrix, i.e. low Sn concentration in the matrix (other factors being equal). Higher n values indicate greater matrix diffusion and limitations arising from the diffusion through the Nb_3Sn layer. Values of n close to one again imply the reaction at the Nb/Nb_3Sn interface is the limiting step (15).

The LBL wires have high n values, n=0.6, significantly higher than the value seen for the Hitachi wire, n=0.2. This anomalous behaviour results from the extremely high Sn supply in these wires. Diffusion through the matrix is more than adequate and the limiting step is the Sn diffusion through the existing Nb_3Sn.

The Hitachi wire, with its n value of 0.2 is much more representative of commercial wires. In this case, it is believed that the Sn diffusion rate within the matrix is limited. The lower matrix Sn supply creates a lower driving force for diffusion and hence a lower n value.

B. SEM vs. TEM

A large portion of the microstructural information is obtained through SEM imaging of fracture surfaces. The fractured wire cross-sections readily reveal the residual Nb, the reacted Nb_3Sn and the bronze matrix. The brittle superconducting phase undergoes predominantly intergranular fracture, and hence grain size and other morphological information is available. Additionally, the interfaces between the various phases are easily observed. This technique is especially advantageous in that the entire wire cross-section is intact during viewing. It is possible to establish, unambiguously, the exact location within the wire cross-section as well as location within an individual filament. With proper specimen preparation and mounting in the microscope, resolution at high magnifications as good as that achieved in the transmission electron microscope is possible.

However, TEM results are more accurate than those obtained through SEM analysis. TEM images unambiguosly reveal grain boundaries; the

presence of a favorable fracture mode is not necessary to distinguish grain edges. For example, grains straddling low-angle grain boundaries may cleave together; in the resulting SEM image this appears as the fracture of a single grain. In this respect, TEM results are superior.

Unfortunately TEM specimen preparation is difficult. The different ion milling behaviors of the component materials hinder the preparation of specimens containing all three, even two of the three, phases. Information regarding the phase interfaces is thus not readily available. Furthermore, due to the small viewing area available in a TEM specimen, it is hard to establish the viewing location within a filament and within the wire itself.

The microstructural study performed in this work requires a large data base, i.e. a large number of specimens, an impractical task given the difficulty of TEM specimen preparation. Consequently, this study includes a comparison of microstructural information obtained from both TEM and SEM techniques. Microstructural features seen with SEM and TEM are similar, Fig. (III-12) and Figs. (III-2) and (III-3), Fig. (III.13) and hence the SEM technique can be used, in this case, to accurately determine the microstructure.

C. Microstructure Development

The microstructural observations presented here establish that Nb_3Sn growth occurs as columnar grains. With Nb_3Sn layer growth a shell of equiaxed grains appears between the columnar grained region and the bronze matrix. Grain size within this region is smallest nearest the columnar grains, where grain diameter is approximately equal to the short transverse length of columnar grains, and increases

with proximity to the bronze matrix. Continued growth of the Nb_3Sn layer is accomplished as an increase in the extent of the equiaxed shell; fully reacted wires exhibit the largest volume fraction of equiaxed grains. In fact, fully reacted LBL wires exhibit a solely equiaxed microstructure. This anomalous behavior of the LBL wires is accompanied by extremely fast formation rates of the superconducting phase.

Microstructural development in multifilamentary Nb_3Sn composites has been studied in the past, and two mechanisms have been proposed. The first explains the observed microstructure in terms of a competition between growth of existing grains and nucleation of new grains (17). Alternately, it is hypothesized that a stress induced grain break-up is responsible for the unique morphology (18-21).

Details of the first proposal, Suenaga et al. are as follows: A high matrix Sn concentration results in a high Sn flux and therefore high Sn concentration at the Nb/Nb_3Sn interface. Hence, the driving force for nucleation is high. Many Nb_3Sn grains nucleate and an equiaxed grain structure results. Similar reasoning implies that high temperatures, which correspond to high Sn mobility, also result in an equiaxed morphology. For low Sn concentrations, the Sn flux and subsequent concentration at the interface is lower; the driving force for nucleation is reduced, and growth of the Nb_3Sn layer occurs primarily by growth of existing grains. Similarly, at lower temperatures and less atomic mobility, growth of existing grains occurs. Both situations lead to a columnar morphology.

The above approach agrees with observed final microstructures; high-Sn LBL wires are equiaxed and the low-Sn Hitachi wire exhibits

columnar grains. However, experimental observation on partially reacted wire shows that columnar grains are always present at the Nb/Nb_3Sn interface; i.e. Nb_3Sn always forms as columnar grains. For thin reacted layers, columnar growth is observed in all wires regardless of reaction temperature and matrix Sn concentration, contrary to the above proposal.

The stress induced grain break-up mechanism was first proposed by Wu et al. (18). A volume increase, approximately 35%, accompanies the formation of Nb_3Sn from Nb and a Cu-Sn matrix. The predicted magnitude of the stresses created by this transformation to Nb_3Sn far exceed its yield stress (21), yet the Nb_3Sn layer is intact. Alternate relief mechanisms must be operative and are held responsible for the observed microstructure. Observations by Wu et al., include the presence of dislocations near the outer periphery (farthest from the Nb core) of the columnar grains. And, for equiaxed grains nearest the columnar layer, low angle grain boundaries and grain diameter equal to the short transverse dimension of the columnar grains. Wu et al. proposed that the induced stresses are high enough to nucleate and subsequently polygonize dislocations in the columnar grains, effectively breaking up the columnar grains into equiaxed grains. Subsequent grain growth accounts for the increase in equiaxed-grain size with proximity to the Cu-Sn matrix.

Evetts and co-workers further calculate a stress distribution within the reacted layer. In this model, the tangential stress increases radially out from the Nb core. A critical stress level is reached at some radius and initiates the decomposition of columnar grains. Thus a critical columnar-grained layer thickness is predicted.

Further stress relief is provided by grain boundary sliding and grain rotation.

Both approaches, Wu and Evetts, account for the observed microstructures. The columnar grains are apparently decomposing. The temperature dependence of microstructure is also justified. Dislocation mobility increases with temperature, making columnar grain break-up via a dislocation flow mechanism easier. Shorter columnar grains are observed with an increase in temperature, e.g. Fig. (III-9). The Hitachi wire, and other similarly processed low R wires, always exhibit a columnar-grained layer throughout the whole transformation process. However, this is not true for the LBL wires where the final microstructure is all equiaxed.

Evidence presented here supports the hypothesis that the observed microstructure is a result of a stress induced break-up of columnar grains. Furthermore, this work finds that altering the stress rate, i.e. altering the Nb_3Sn growth rate, changes the final microstructure. Hence both time dependent and time independent stress relief mechanisms are active, e.g. diffusional processes and dislocation flow, respectively.

Nb_3Sn layers formed under high stress rates (fast growth rates) reach the critical stress level quickly. Time dependent mechanisms which operate in the slow growth wires reduce the stress rate and thicker columnar grained layers are thus expected. For the same stage of reaction, the extent of the columnar grained region is larger for the slow-growth Hitachi wire than for the fast-growth LBL wire. In fact, the columnar grained region completely disappears in the LBL wires.

C. Effect of Dopants

The dopants, Ti and Mg, are added to improve current carrying capacity. It is expected that the Ti will change the inherent superconducting properties of the Nb_3Sn, while the Mg will predominantly affect microstructure.

Microstructural development in the doped wires is similar to the undoped wire. Initially, columnar growth occurs at the Nb/Nb_3Sn interface. For thick Nb_3Sn layers an equiaxed morphology exists. Grain size is qualitatively similar for all wires. Layer growth is slightly greater for the doped than for the undoped wire. The reasons are not understood but this behavior is in accordance with other results (27,28).

The inherent properties of the Ti doped Nb_3Sn phase, as measured by the H_{c2}^*, are superior to that of the undoped wire. An increase of 5T in H_{c2}^* is observed at 14T. This increase accounts for the higher J_c of this wire. These results are consistent with those reported elsewhere (25-28).

Past work on Mg additions to the Nb_3Sn phase predicts a grain refining effect (22-24). It is well known that the J_c increases as grain size decreases (1), and thus an increase in J_c is expected with Mg addition. Prior work on similarly processed Mg doped wires confirms this (24). However, the Mg doped wires studied in this work do not show an increase in J_c. Microstructural investigation reveals that no grain refinement accompanies the Mg addition and hence, no increase in Jc should be expected.

As discussed earlier, the LBL doped wires have very high bronze to niobium ratios and hence fast growth rates. The fast growth rate, in itself, exerts a refining influence on the microstructure. The mechanism of grain refinement in Mg doped wires is not well understood. This work indicates that once a fine equiaxed microstructure is achieved, further refinement as a result of dopants cannot be detected. In fact it appears that the dopants, in this case, are detrimental to the wire. The manufacturability of the wires is greatly reduced by the Mg addition and more processing steps are necessary. Specifically, increased frequency of intermediate anneals at higher temperatures is needed, steps which harm the final microstructure of the wire (31).

V. CONCLUSIONS

1) Columnar Nb_3Sn grains are present adjacent to the Nb interface for all initial Nb_3Sn layer thicknesses.

2) Stress relief mechanisms, operating to relieve stresses induced by the transformation of Nb to Nb_3Sn, are predominantly responsible for the microstructure of the reacted layer. Both time dependent (diffusive) and time independent (non-diffusive) mechanisms operate. Thus the Nb_3Sn formation rate affects the final microstructure. A fast formation rate results in an equiaxed morphology.

3) The addition of Mg to the starting Cu-Sn in bronze-route multifilamentary conductors refines the final Nb_3Sn microstructure effecting higher critical current densities, Wu et al. However, the grain refining effect, and concommitant increase in J_c, is indiscernible when the Nb_3Sn formation rate is such that a fine equiaxed morphology results.

4) The addition of Ti to the starting Nb in bronze-route multifilamentary conductors raises the H_{c2}^* of the Nb_3Sn and thus the critical current densities, with no accompanying impact on the microstructure.

5) Accurate grain size and shape determination within the Nb_3Sn layer is possible through SEM examination of fractured wire surfaces.

VI. REFERENCES

1. R. M. Scanlan, W. A. Fietz, E. F. Koch, J. Appl. Phys., 46, p. 2244 (1975).

2. B. J. Shaw, J. Appl. Phys., 47, p. 2143 (1976).

3. J. D. Livingston, Phys. Stat. Sol. (a), 44, p. 295 (1977).

4. G. Zerweck, J. Low. Temp. Phys., 42, p. 1 (1981).

5. E. J. Kramer, Adv. Cryo. Eng., 28, p. 307 (1982).

6. B. E. Jacobsen, R. H. Hammond, T. H. Geballe, J. R. Salem, J. Less Common Metals, 62, p. 59 (1978).

7. T. P. Orlando, J. A. Alexander, S. J. Bending, J. Kwo, S. J. Poon, R. H. Hammond, M. R. Beasley, E. J. McNiff, S. Foner, IEEE Trans. Mag., MAG-17, p. 368 (1981).

8. D. B. Smathers, D. C. Larbalestier, Filamentary A15 Superconductors, edited by M. Suenaga and A. F. Clark (Plenum Press, New York, 1980).

9. E. J. Kramer, J. Appl. Phys., 44, p. 1360 (1973).

10. G. Rupp, E. Springer, S. Roth, Cryogenics, 17, p. 141 (1977).

11. M. Suenaga, T. Onishi, D. O. Welch, T. S. Luhman, Bull. Am. Phys. Soc., 23, p. 229 (1978).

12. M. Suenaga, D. O. Welch, Ref. 8, p. 132.

13. A. R. Kaufmann, J. J. Pickett, Bull. Am. Phys. Soc., 15, p. 833 (1970).

14. B. V. Reddi, S. Ray, V. Raghavan, A. V. Narlikar, Phil. Mag. A 38, p. 559 (1978).

15. S. K. Agarwal, S. B. Samanta, V. K. Batra, A. V. Narlikar, J. Mater. Sci., 19, p. 2057 (1984).

16. B. V. Reddi, V. Raghavan, S. Ray, A. V. Narlikar, J. Mater. Sci., 18, p. 1165 (1983).

17. S. Okuda, M. Suenaga, R. L. Sabatini, J. Appl. Phys, 54, p. 289 (1983).

18. I. W. Wu, D. R. Dietderich, J. T. Holthuis, M. Hong, W. V. Hassenzahl, J. W. Morris, Jr., J. Appl. Phys., 54, p. 7139 (1983).

19. J. R. Cave, C. A. F. Weir, IEEE Trans. Mag., MAG-19, p. 1120, (1983).

20. N. J. Pugh, J. L. M. Robertson, E. R. Wallach, J. R. Cave, R. E. Somekh, J. E. Evetts, IEEE Trans. Mag., MAG-21, p. 1129 (1985).

21. E. R. Wallach, J. E. Evetts, Adv. Cryo. Eng., 32, to be published.

22. K. Tachikawa, Adv. Cryo. Eng., 26, p. 378 (1980).

23. K. Togano, T. Assano, K. Tachikawa, J. Less Common Metals, 68, p. 15 (1979).

24. I. W. Wu, D. R. Dietderich, et al., Appl. Phys. Lett. 45(7), p.792 (1984).

25. K. Tachikawa, T. Asano, T. Takeuchi, Appl. Phys. Lett. 39(9), p. 766 (1981).

26. K. Tachikawa, H. Sekine, Y. Iijima, J. Appl. Phys., 53(7), p. 5354 (1982).

27. K. Kamata, N. Tada, K. Itoh, H. Tachikawa, IEEE Trans. Mag., MAG-19, p. 1429 (1983).

28. H. Sekine, Y. Iijima, K. Itoh, K. Tachikawa, Y. Tanaka, Y. Furuto, IEEE, Trans. Mag., MAG-19, p. 1429 (1983).

29. H. H. Farrell, G. H. Gilmer, M. Suenaga, J. Appl. Phys., 45, p. 4025 (1974).

30. P. E. Johson-Walls, D. R. Dietderich, et al., IEEE Trans. Mag., MAG-21, p. 1137 (1985).

31. D. B. Smathers, K. R. Marken, D. C. Larbalestier, R. M. Scanlan, IEEE Trans. Mag., MAG-19, p. 1417 (1983).

32. T. Luhman, D. Dew-Hughes (eds.), Treatise on Materials Science and Technology, 14 p. 236, Academic Press, New York, (1979).

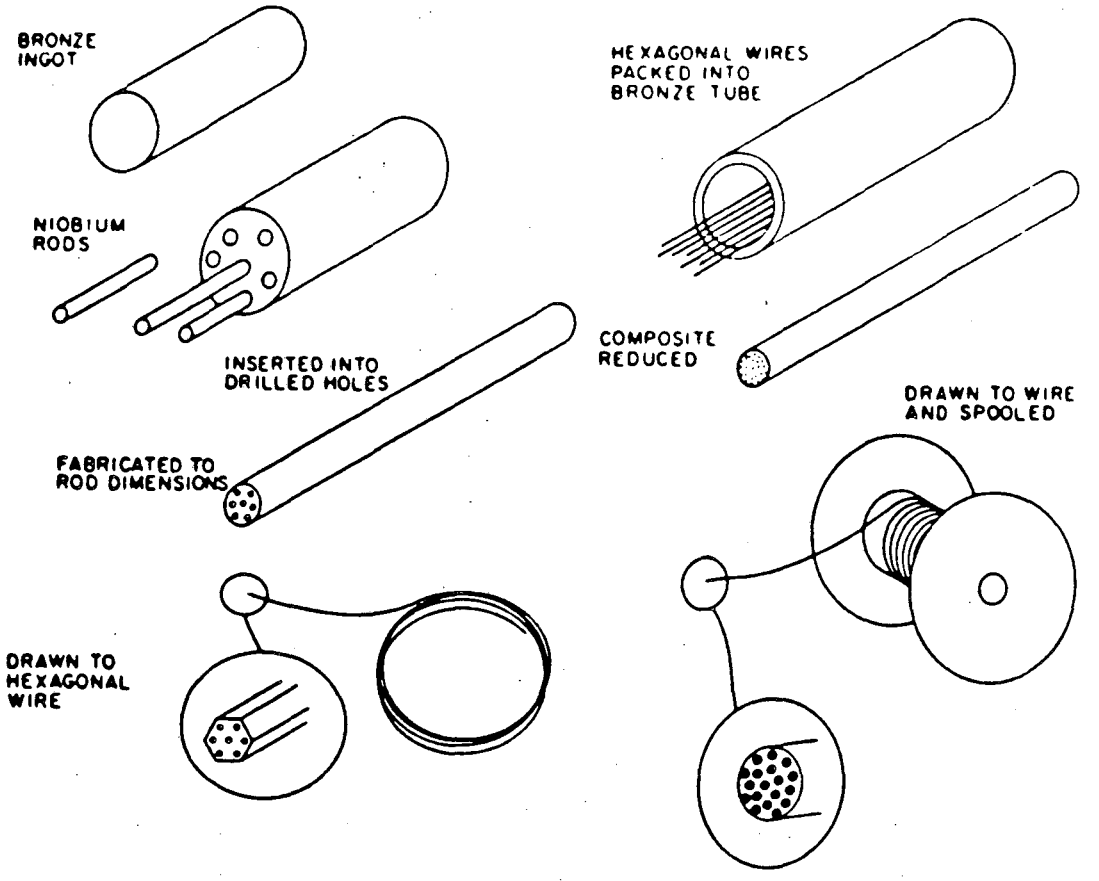

Fig. I-1. Schematic representation of the "bronze process" multifilamentary conductor route (32).

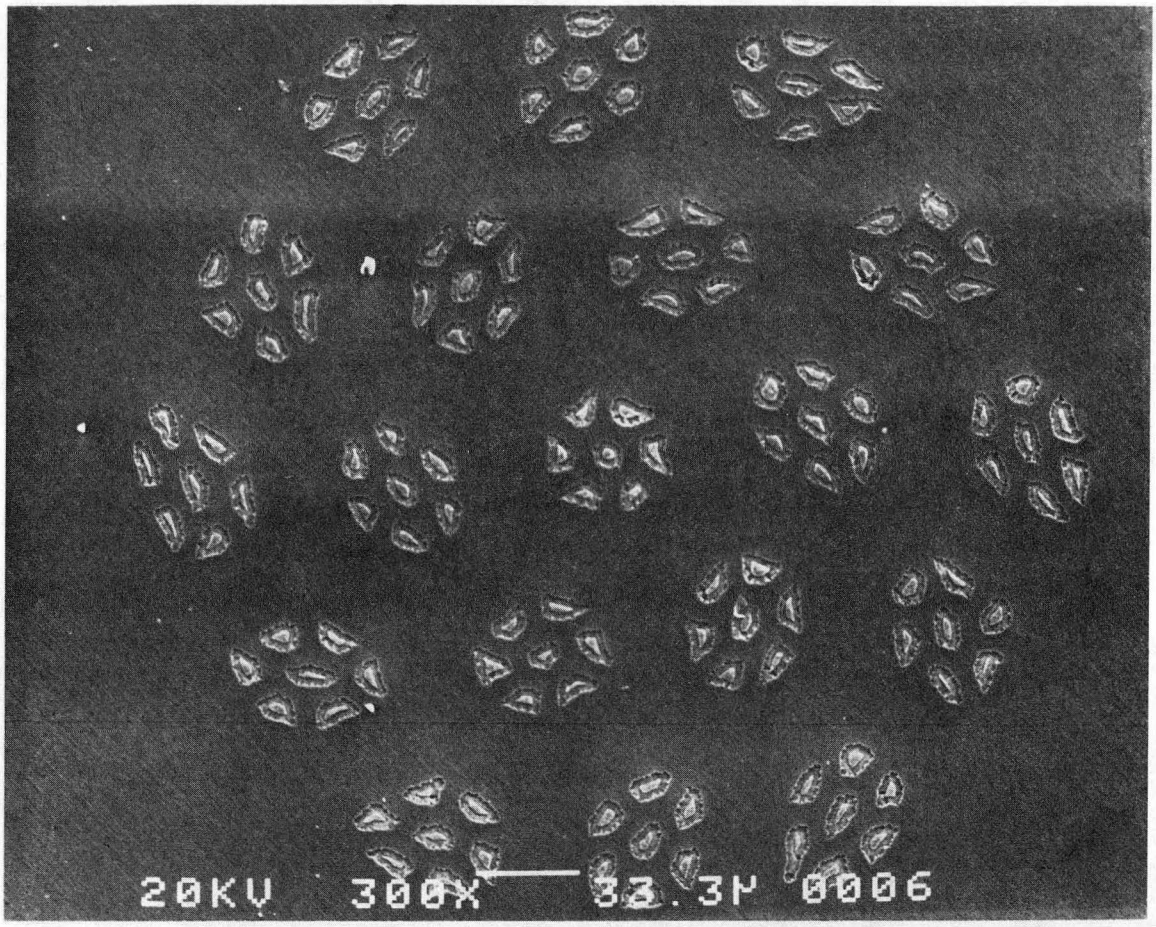

XBB 848-5761

Fig. II-1. Scanning electron micrograph of a partially reacted LBL wire showing Nb/Nb_3Sn filament configuration.

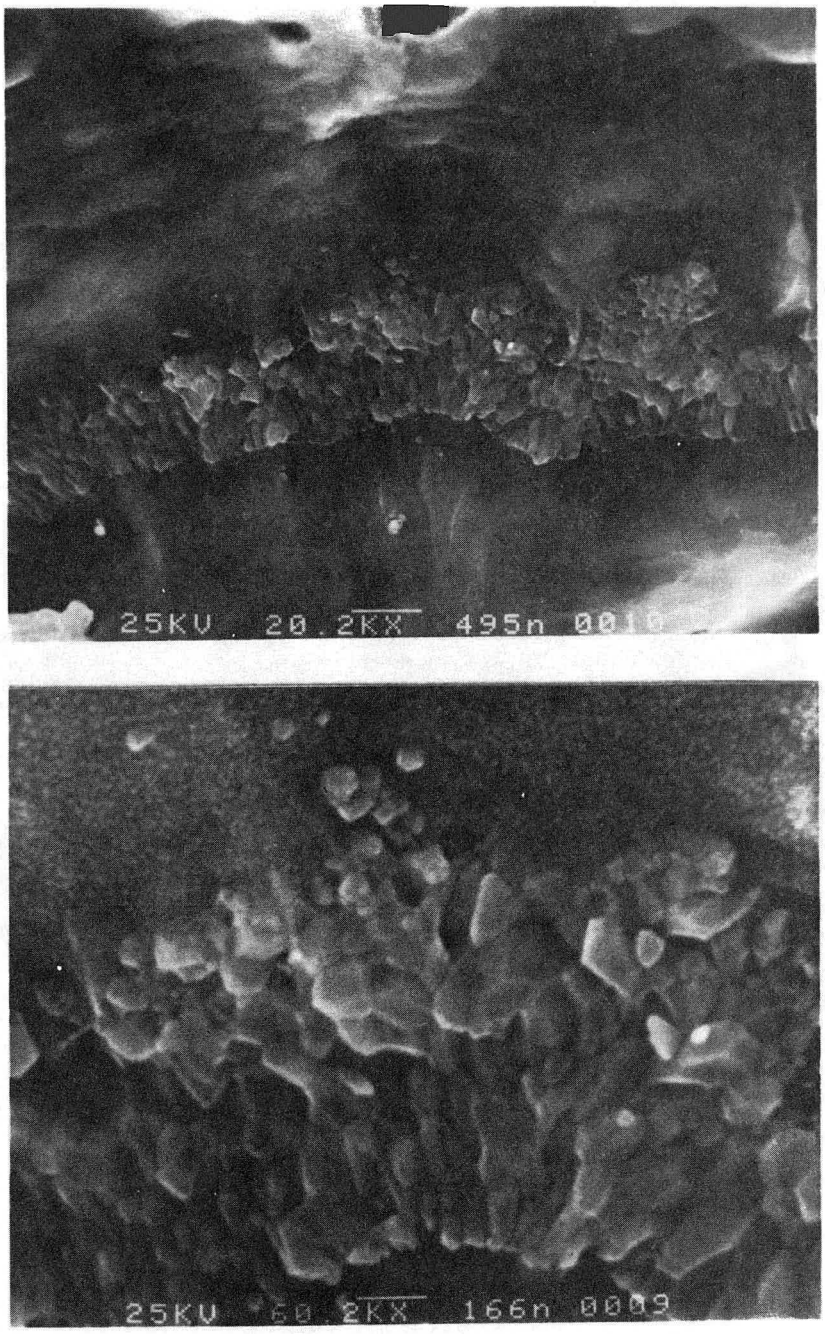

XBB 858-6931

Fig. III-1. SEM fractograph of an LBL wire reacted at 700°C/6hours. Columnar grains are visible at the Nb/Nb_3Sn interface, equiaxed grains comprise the balance of the Nb_3Sn layer. Grain diameter of the equiaxed grains nearest the columnar layer is approximately equal to the short transverse dimension of the columnar grains.

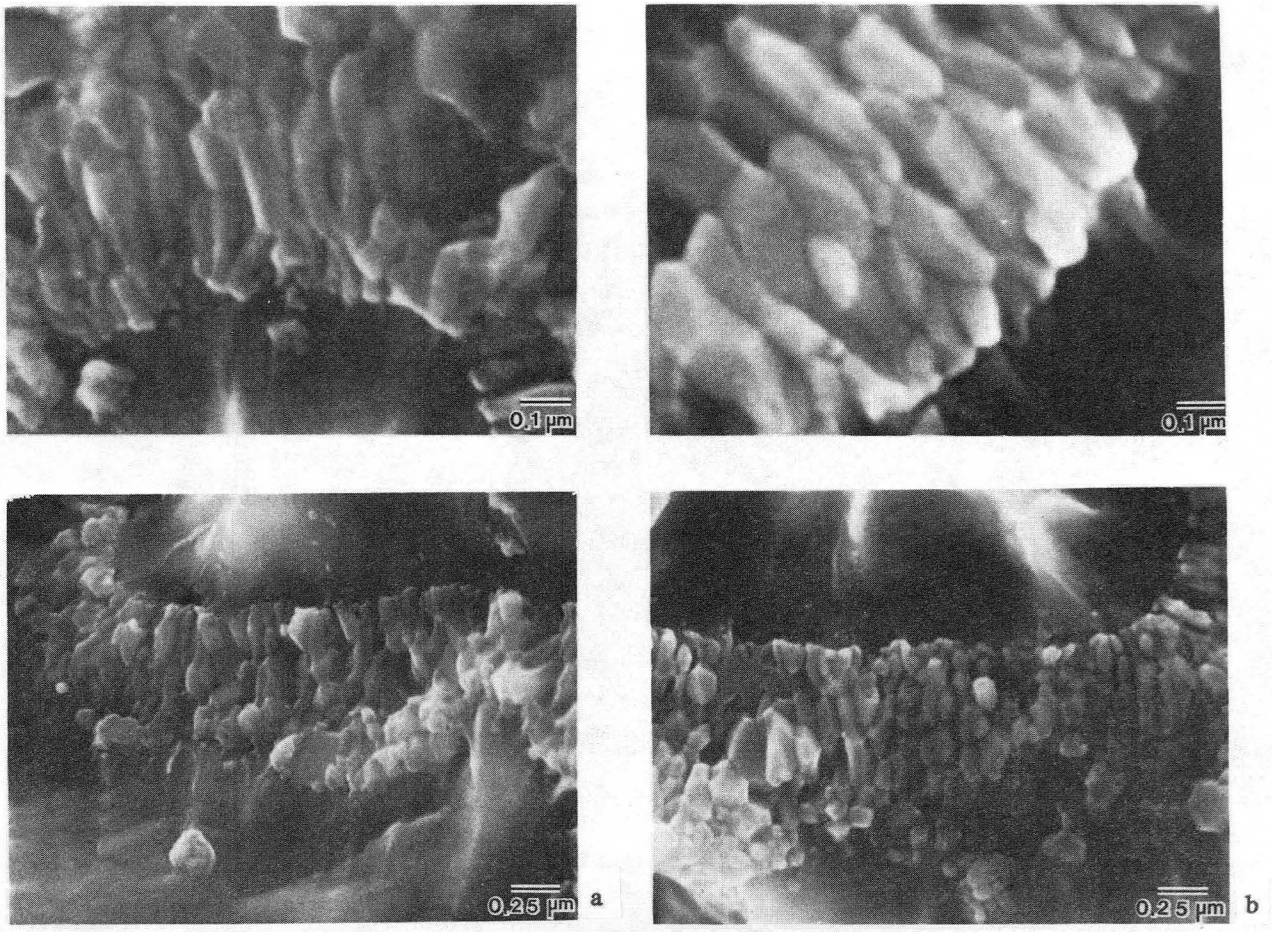

Fig. III-2. SEM fractographs of LBL wire reacted at 700°C/6hours (a) and 700°C/12hours (b). For both heat treatments columnar grains are visible at the Nb/Nb_3Sn interface. The aspect ratio of the columnar grains decreases with longer heat treatments.

XBB 861-736

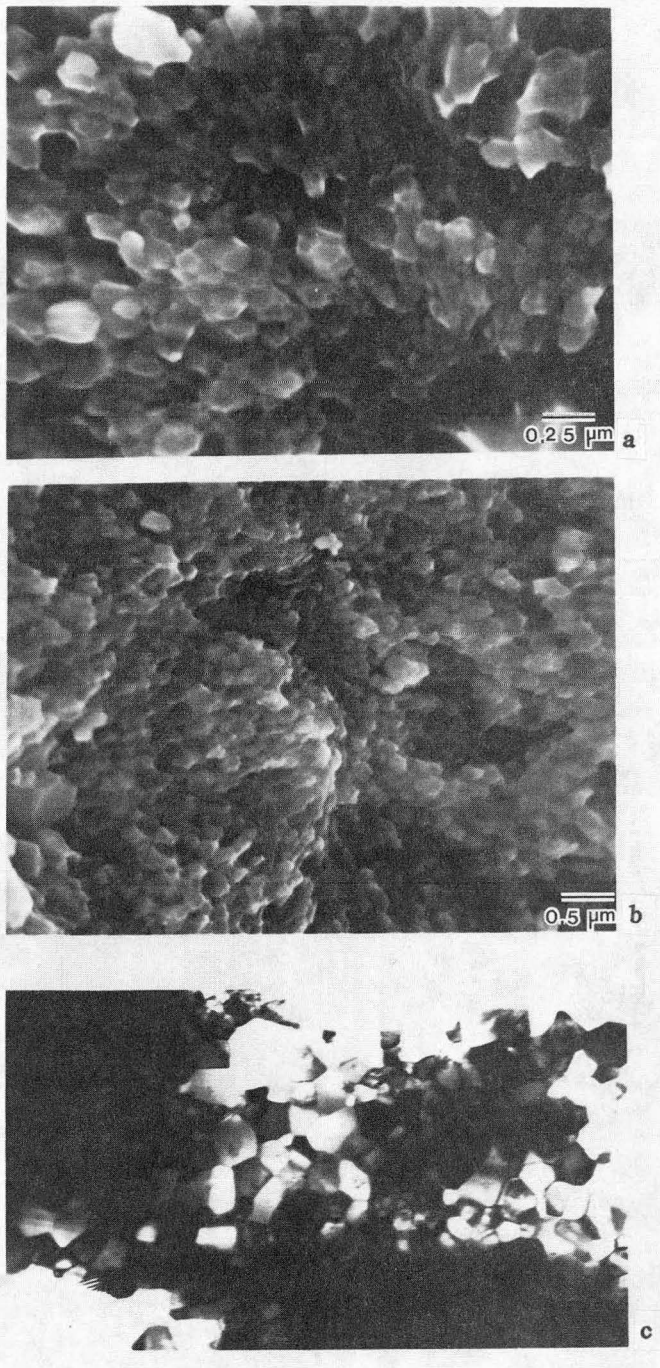

Fig. III-3. LBL wire reacted at 700°C/3days (a) and 700°C/7days (b). Only equiaxed grains are present. In (b), all Nb has been consumed; grain morphology remains equiaxed. (c) TEM micrograph of specimen in (b). Similar features are seen.

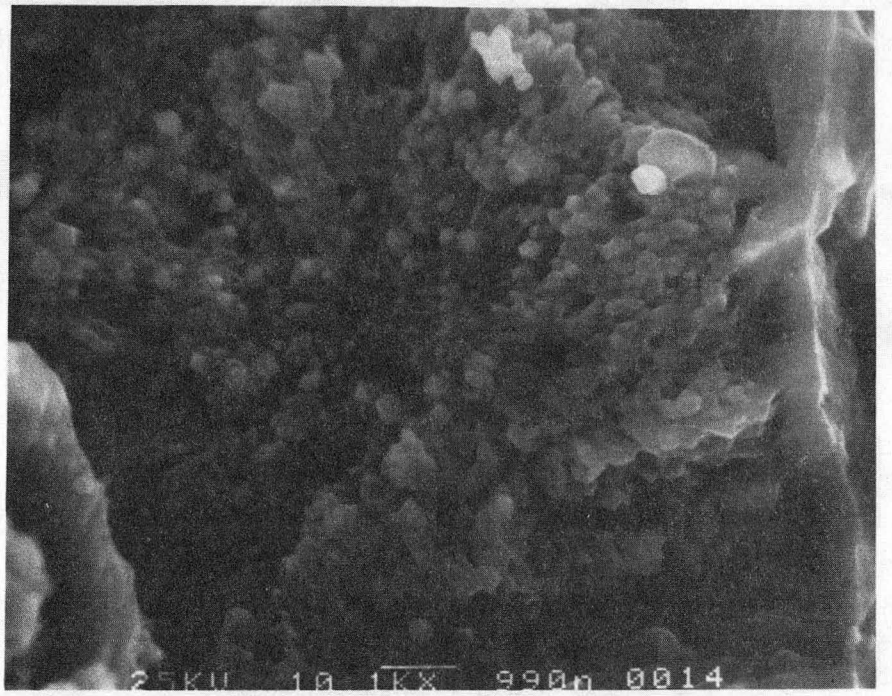

XBB 863-1905

Fig. III-4. SEM fractograph of LBL wire reacted at 780°C/1day. All Nb has been consumed. Reacted layer is composed of equiaxed grains only.

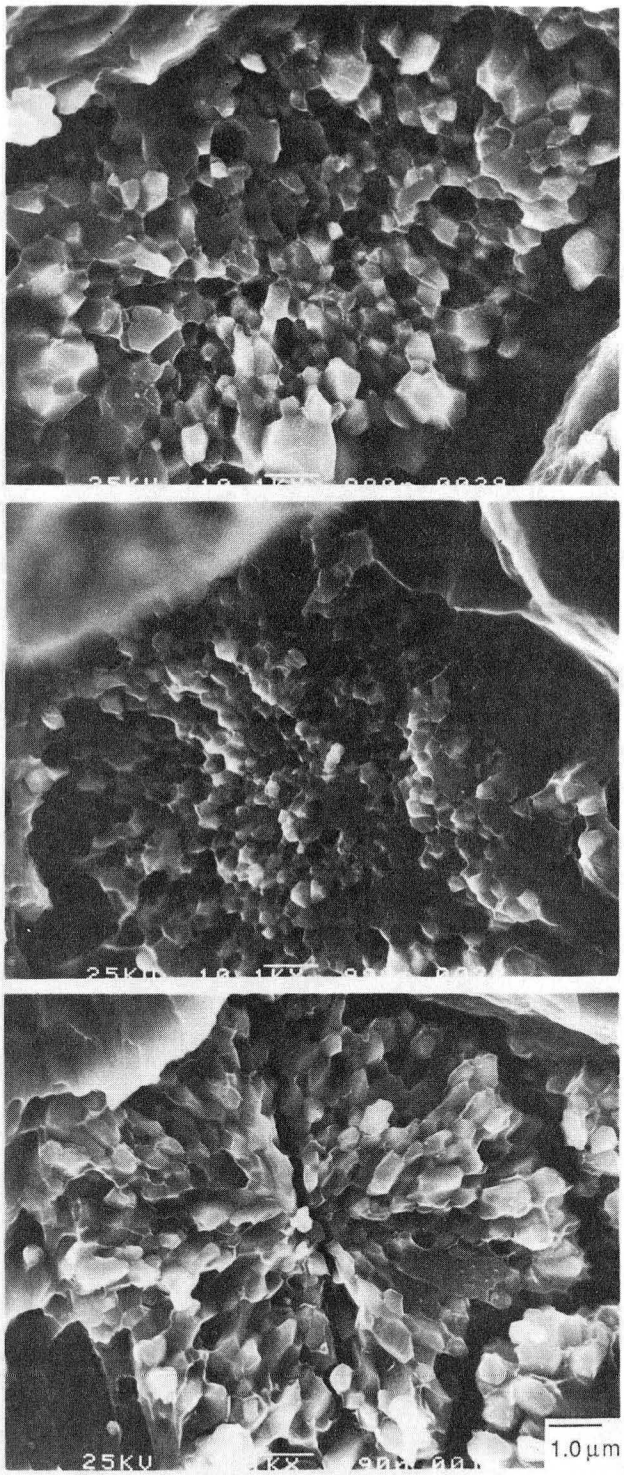

XBB 864-2704

Fig. III-5. SEM fractographs of LBL doped wires (700°C/6hours). Wire doped with Mg (a), doped with Ti (b), and control (undoped) wire (c). All specimens exhibit columnar grains directly at the Nb/Nb_3Sn interface.

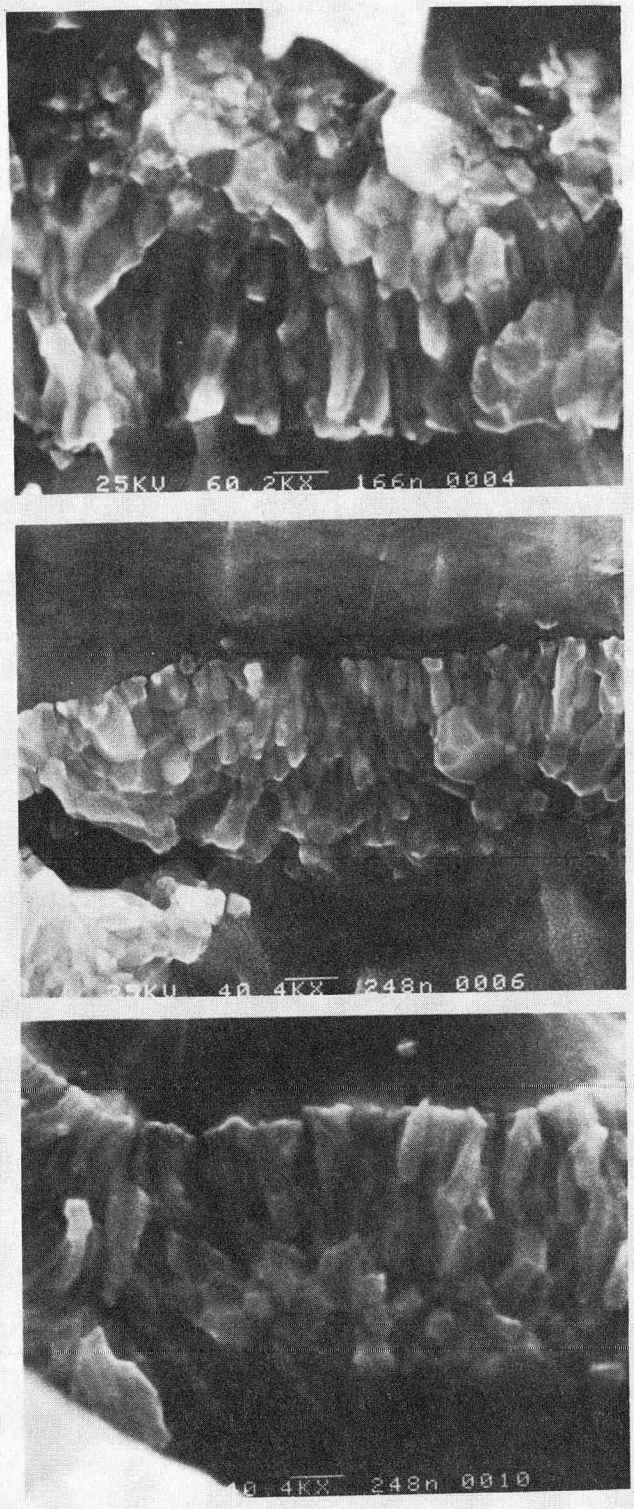

Fig. III-6. SEM fractographs of fully reacted LBL wires (780°C/4days). Ti doped wire (a), Mg doped wire (b), and control (undoped) wire (c). All wires exhibit similar, equiaxed morphologies at full reaction.

XBB 863-1906

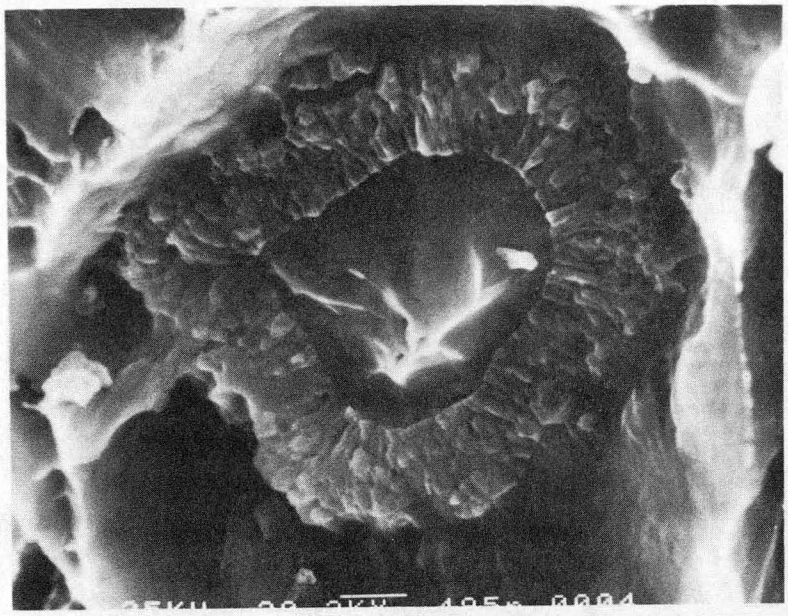

0.5 μm

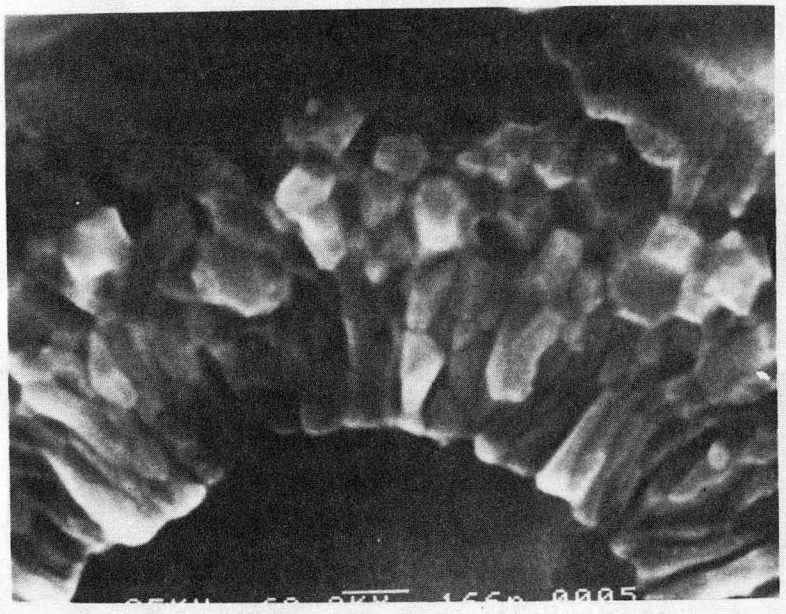

0.17 μm

XBB 863-1904

Fig. III-7. SEM fractographs of Hitachi wire reacted at 700°C/15hours. Columnar grains of high aspect ratio are visible at the Nb/Nb_3Sn interface. Equiaxed grains comprise the balance of the reacted layer.

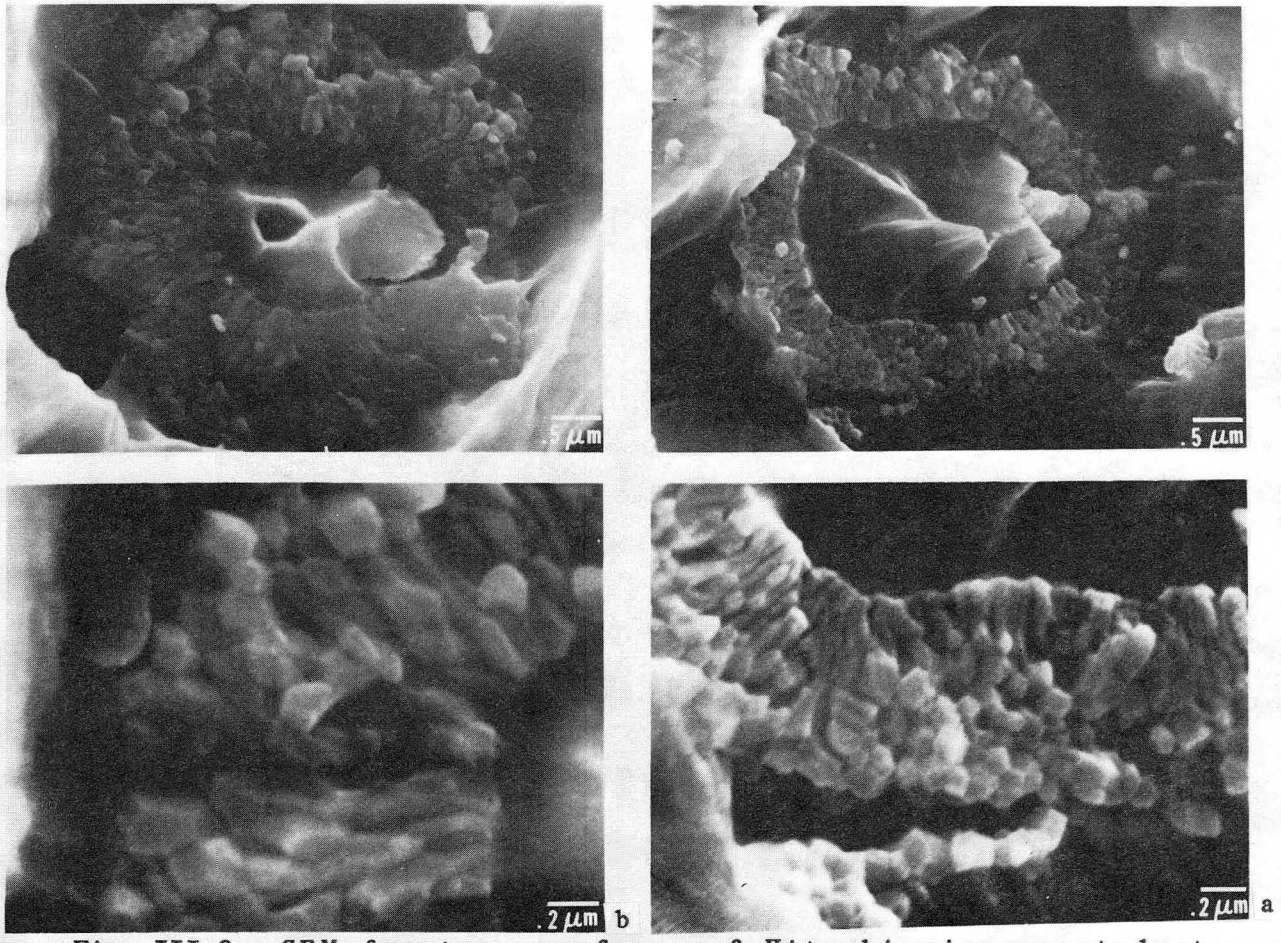

Fig. III-8. SEM fracture surfaces of Hitachi wire reacted at 700°/7hours (a) and 700°C/7days (b). Columnar grains are visible at the Nb/Nb_3Sn interface for both reaction treatments. Layer growth occurs as an increase in both the columnar and equiaxed regions.

XBB 849-6702

a

0.17 μm

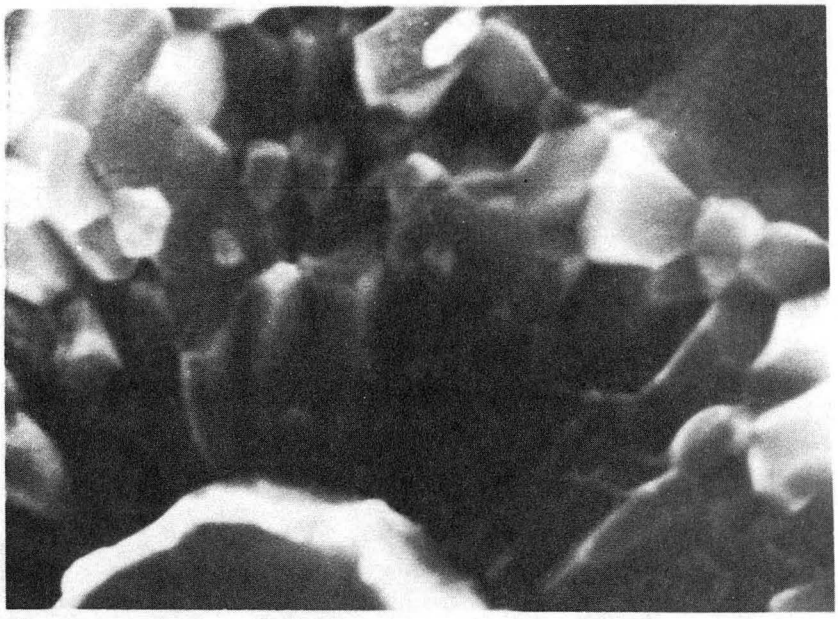

b

0.17 μm

XBB 863-1903

Fig. III-9. SEM fractographs of Hitachi wire reacted at 700°C/7days (a) and 750°C/4days (b). Columnar grains are visible adjacent to the unreacted Nb core. The aspect ratio of the columnar grains is higher for the lower temperature reaction.

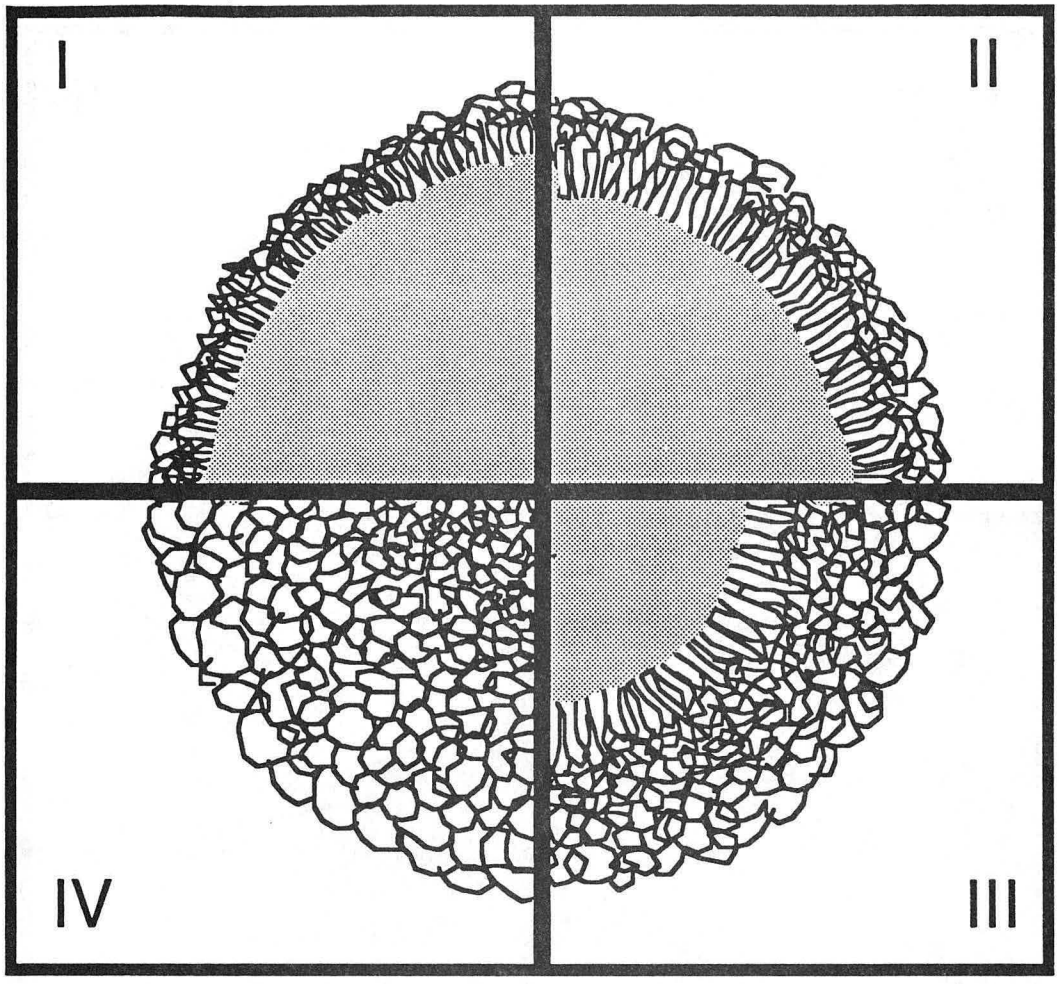

Fig. III-10. Schematic diagram of Nb_3Sn layer growth in LBL wire. Regions I-IV depict the transformation from outset (I) through full Nb consumption (IV). Thin layers are as in I. A shell of columnar grains at the Nb core is surrounded by a shell of equiaxed grains extending out to the bronze matrix. Equiaxed grain diameter is roughly equal to the short transverse dimension of the columnar grains. Initial layer growth occurs as an increase in both columnar and equiaxed regions, II. On longer reaction, the equiaxed layer comprises most of the reacted cross-section. For fully reacted specimens all columnar grains have decomposed and an equiaxed morphology is present. The shaded central region represents the Nb core.

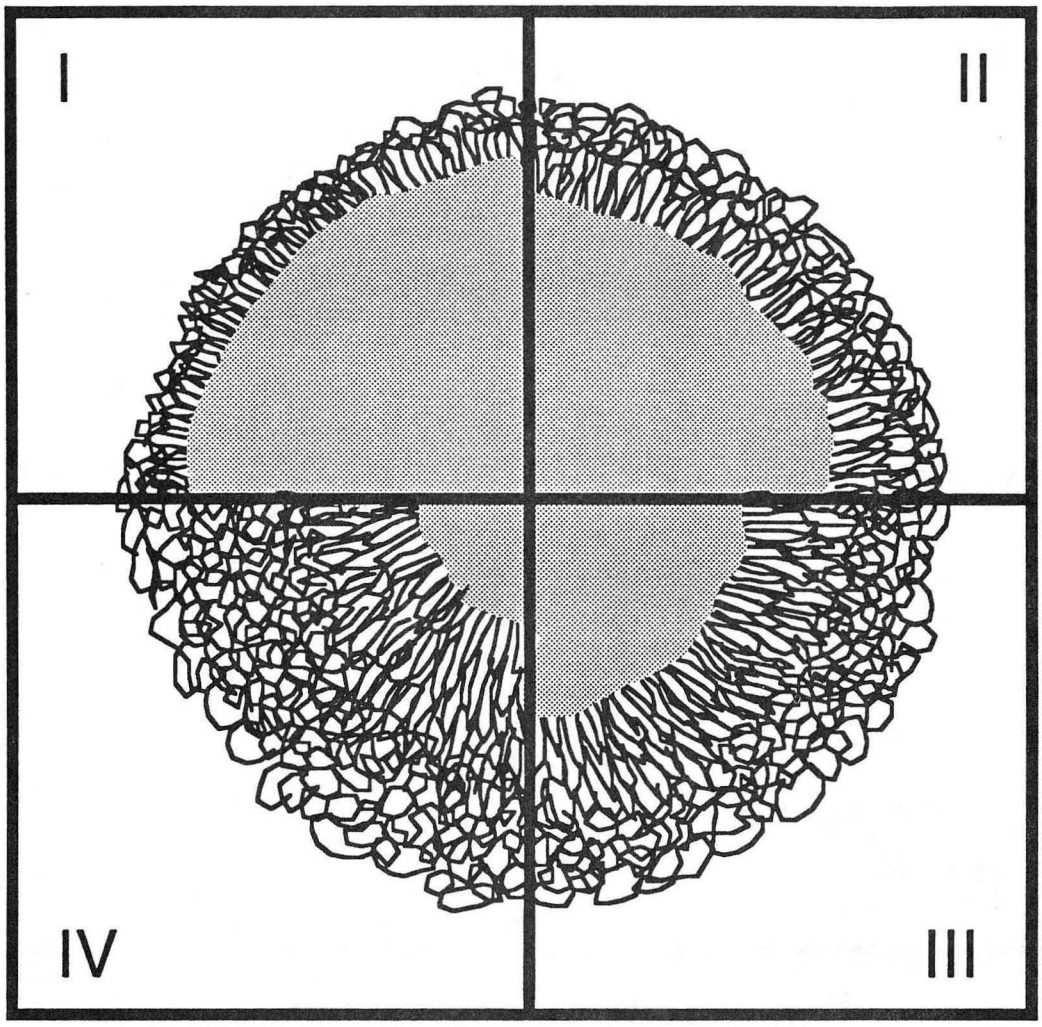

Fig. III-11. Schematic diagram of Nb_3Sn layer growth in Hitachi wire. Regions I-IV depict the transformation from outset (I) through full Nb consumption (IV). Unlike the layer growth in the LBL wire, columnar grains remain at the Nb core through full reaction. (Due to an insufficient supply of Sn, full transformation of the Nb core is not possible.)

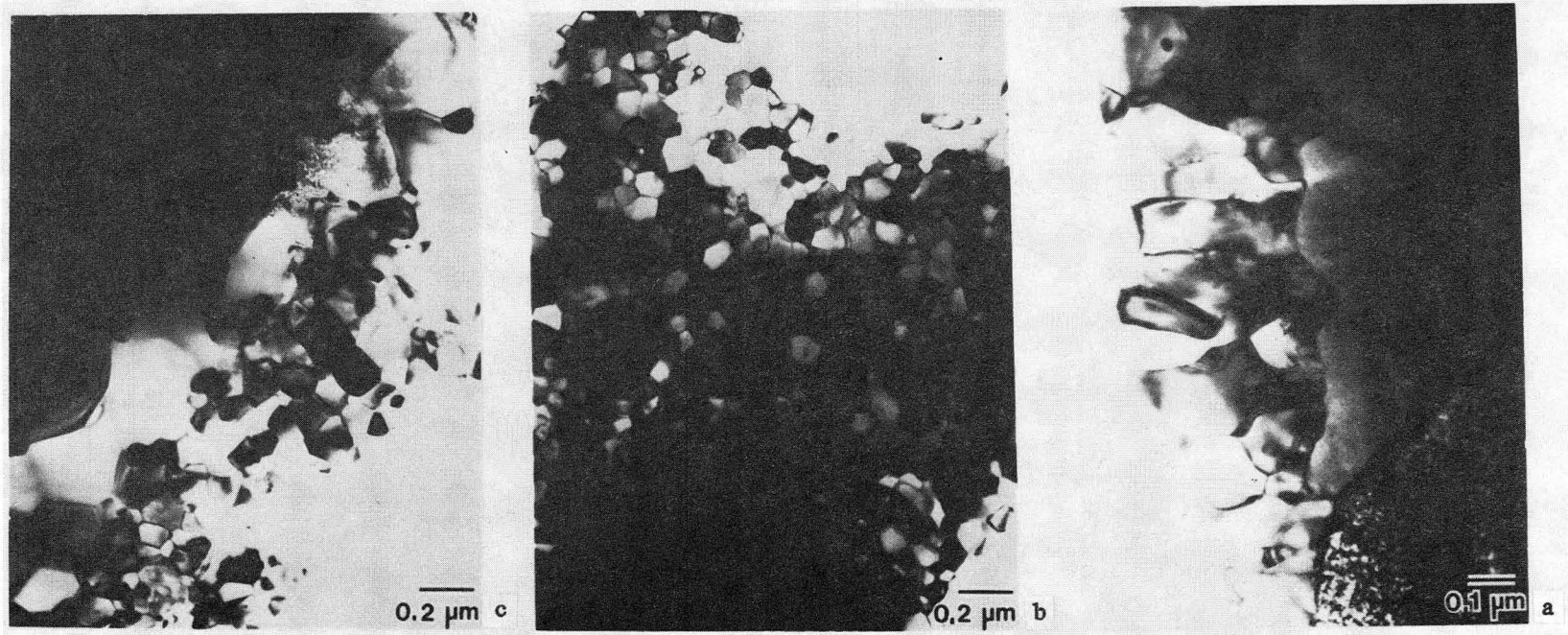

XBB 861-739

Fig. III-12. TEM micrographs of LBL wire reacted at 700°C/6 hours (a) and 700°C/2days (b) and (c). Visible are columnar grains at the Nb core (a), equiaxed region (b), grain size increasing with proximity to the bronze matrix (c).

a

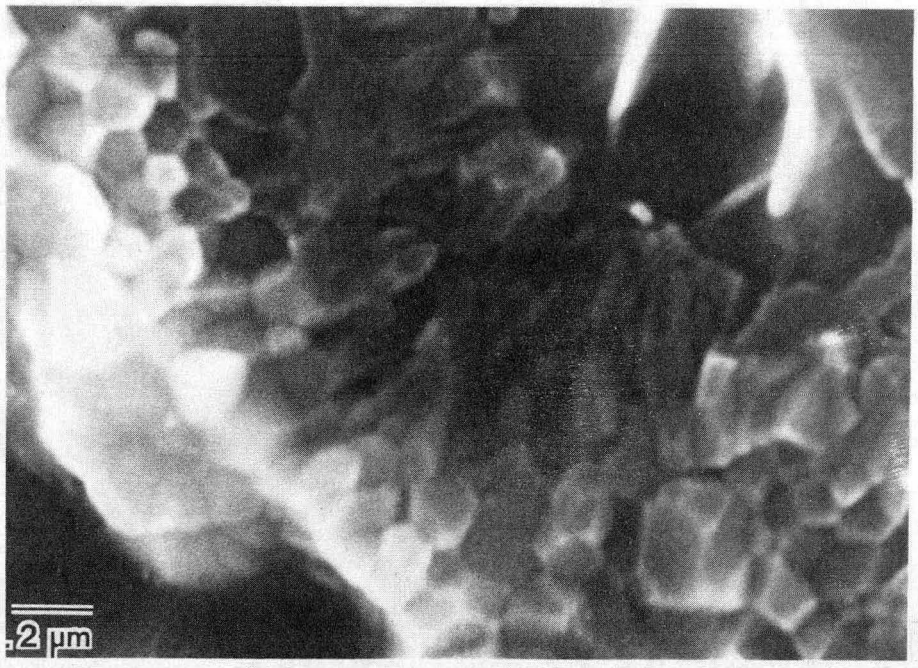

b

Fig. III-13. TEM micrograph of a partially reacted Hitachi wire (a). A cross-sectional view is shown. Columnar grains emanate out from the Nb core, balance of the reacted layer is composed of equiaxed grains. SEM fractograph of the same specimen. Similar morphological features are seen (b).

XBB 849-6569A

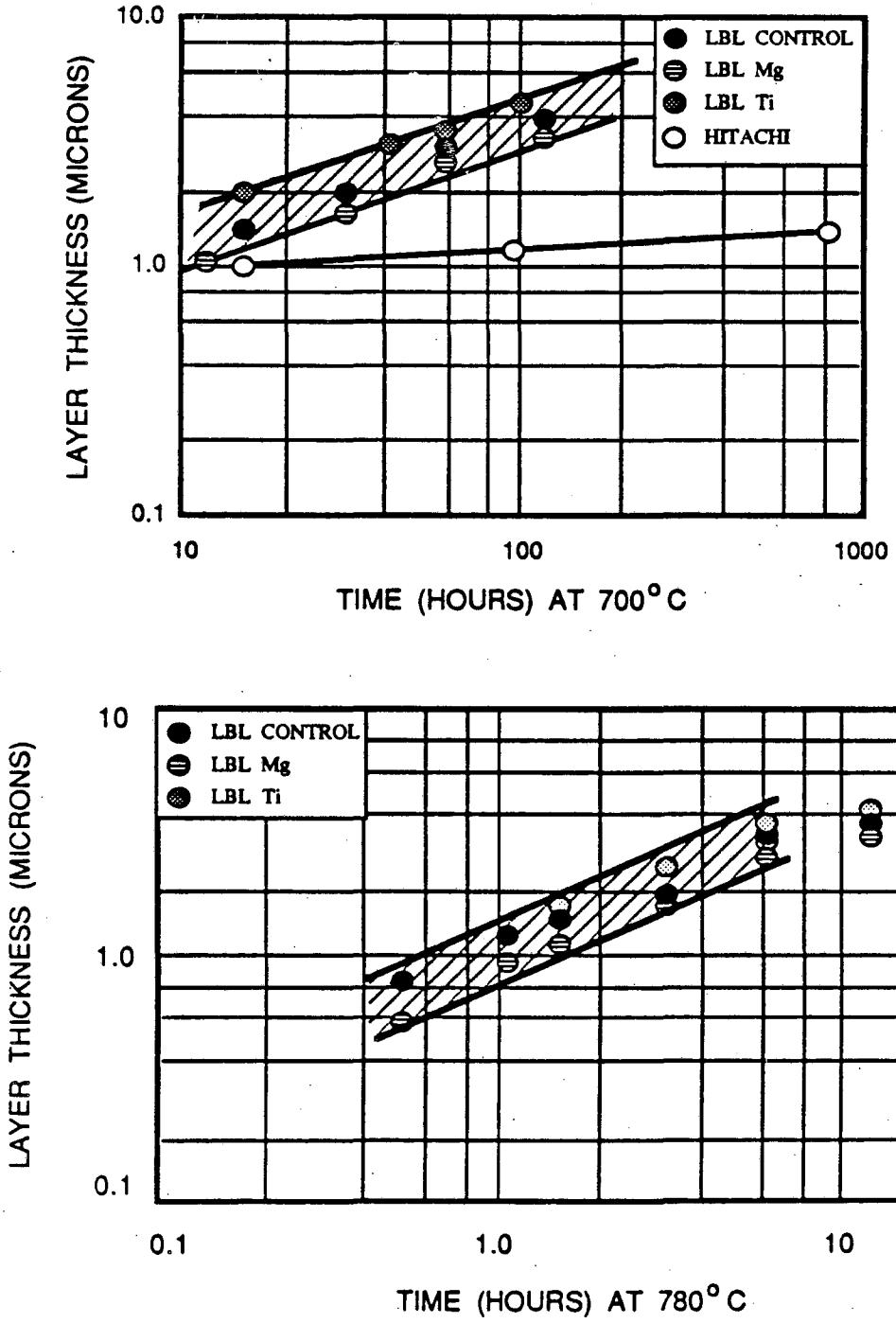

Fig. III-14. Layer thickness vs. reaction time at 700°C and 780°C for all wires studied.

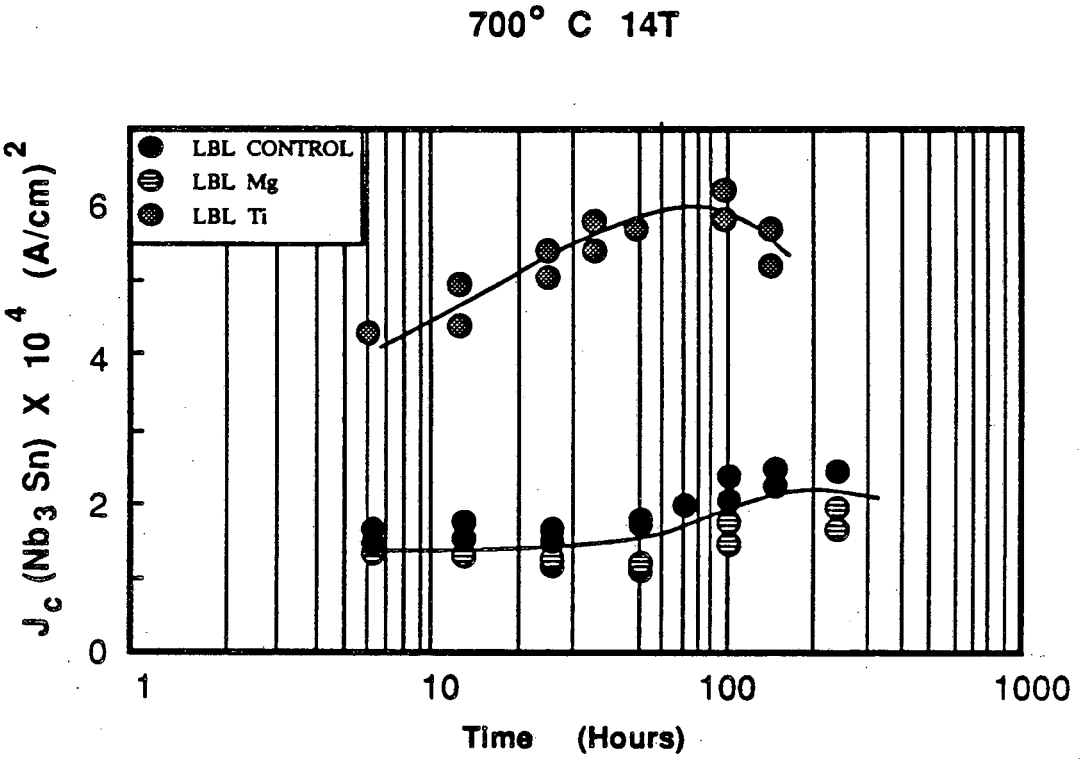

Fig. III-15. Critical current densities at 14T vs. reaction time at 700°C.

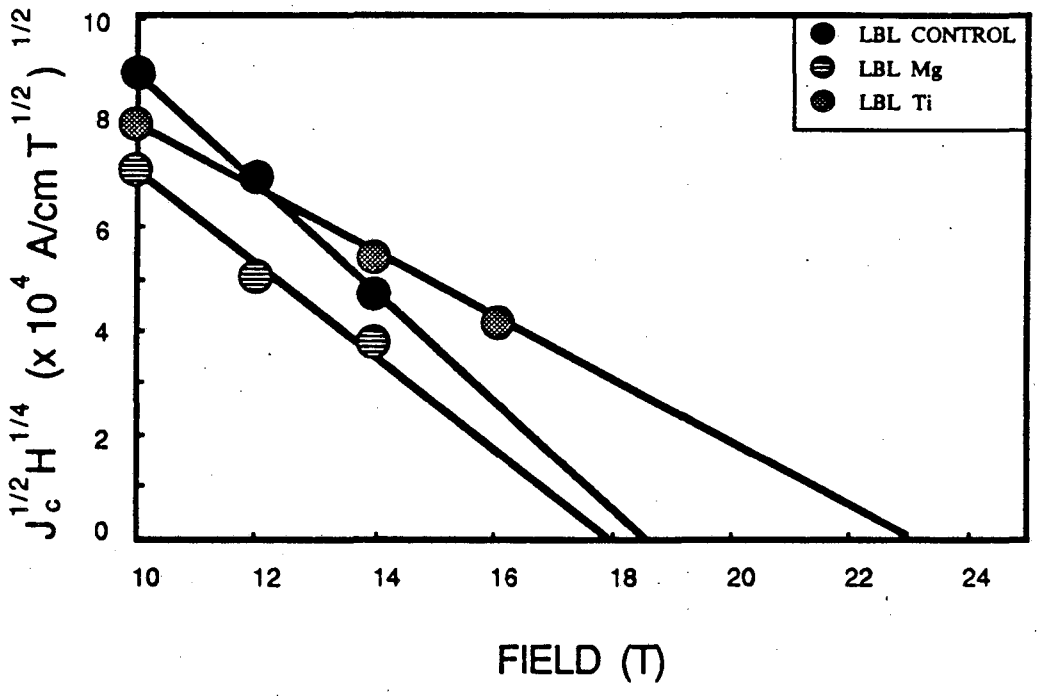

Fig. III-16. Kramer plot. $J^{1/2}H^{1/4}(0)$ is $H_{c2}{}^{*}$.

Table I

Samples Studied

	at% Sn in matrix	R[1]	number of filaments	filament diameter μm	95% at 700° C[2] days
LBL Control	6.7	20	133	9.0	4
LBL Mg[3]	6.7	20	133	9.0	5
LBL Ti[4]	6.7	25	133	9.0	3
Hitachi	6.7	2.5	10,261	4.0	>>8

1. R is the bronze to niobium ratio
2. 95% consumption of Nb core after x days at 700° C
3. 0.2 at% Mg added to bronze matrix
4. 2.0 at% Ti added to Nb core

TABLE II

Time to react 50%, 80%, and 100% of initial Nb

at 780° C (in hours) :

	50%	80%	100%
LBL Control	1	4	20
LBL Mg	1	4	15
LBL Ti	0.5	2	6

at 750° C (in hours) :

	50%	80%	100%
LBL Control	3	6	18
LBL Mg	1.5	5	15
LBL Ti	1.5	5	12
Hitachi	12	>5	

at 700° C (in hours) :

	50%	80%	100%
LBL Control	12	35	150
LBL Mg	15	70	200
LBL Ti	8	20	100
Hitachi	36	>200	

LAWRENCE BERKELEY LABORATORY
TECHNICAL INFORMATION DEPARTMENT
UNIVERSITY OF CALIFORNIA
BERKELEY, CALIFORNIA 94720